*Int. J. Electrochem. Sci.*, 14 **(2019)** 9661 – 9670, doi: 10.20964/2019.10.21

**International Journal of ELECTROCHEMICAL SCIENCE**
www.electrochemsci.org

# Glucose Biosensor Based on Glucose Oxidase Immobilized on Multi-Vacancy $TiO_2$ Nanotube Arrays

*Zhitong Hu, Ju Rong, Zhaolin Zhan, Xiaohua Yu*[*]

School of Materials Science and Engineering, Kunming University of Science and Technology, Kunming 650093, China
[*]E-mail: xiaohua_y@163.com

*Received:* 21 May 2019/ *Accepted:* 23 July 2019 / *Published:* 30 August 2019

$TiO_2$ nanotube arrays (TNAs) are promising low-cost biosensor materials due to their large specific surface area and catalytic activity. Nevertheless, the detection efficiency of TNAs enzymatic glucose biosensors is affected by the amount of glucose oxidase adsorbed and the rate of electron transport. Here, we reveal that the adsorption capacity and electron transport rate of TNAs can introduce more active sites by annealing under an argon atmosphere to form oxygen vacancies, resulting in the generation of highly active surfaces and a significant improvement in the adsorption and conductivity properties. These manufactured highly active TNAs enzymatic glucose biosensors exhibit good electrochemical performance for the oxidation of glucose with a sensitivity of 8.5 $\mu A \cdot mM^{-1} \cdot cm^{-2}$, and a detection limit as low as 3.2 μM. Our study represents a simple method for the preparation of highly stable and selective TNAs enzymatic glucose biosensors by defect engineering, providing a novel concept for the manufacture of other enzyme biosensors.

**Keywords:** $TiO_2$ nanotube arrays, defect engineering, biosensor, electrochemical determination

## 1. INTRODUCTION

Biosensors have attracted considerable attention in recent decades due to their widespread application in medical diagnosis [1], biotechnology [2] and the food industry [3]. In order to detect blood glucose concentration and control diabetes more accurately, research into high-quality glucose biosensors has become a major trend [4,5]. In particular, the development of enzymatic biosensors has drawn extensive attention because of their excellent selectivity, sensitivity and stability [6]. Meanwhile, to solve the problem of enzyme immobilization in enzyme biosensors, nanomaterials, such as gold [7], carbon [8] and titanium dioxide [9] have been studied. In other words, the purpose of enzyme immobilization is to limit the enzyme on the carrier by adsorption and covalent bonding, which improves the stability of the enzyme without affecting its activity [10]. However, the further

development of biosensors is largely limited by the lack of surface active sites of the carrier. Therefore, increasing the surface activity of the carrier has become an important and challenging problem in biosensors.

$TiO_2$ nanotube arrays (TNAs) presenting high specific surface areas have been the focus of intense research owing to their good biocompatibility, photocatalytic properties and immobilization [11–13]. The good stability of $TiO_2$ for enzyme immobilization makes it one of the main carriers of glucose biosensors [14]. The study of $TiO_2$ for glucose biosensors dates back thirty years, but only slow progress has been made because of the poor activity of bulk $TiO_2$ [15]. Nevertheless, interest in this material rose again as a result of the significant increase in the specific surface area of TNAs [16]. Experimental results show that for TNAs, only the surface active sites have high activity on the adsorption of the enzyme, while the base surface is poor [17]. Since then, many studies, including doping and modification, have been made to improve the adsorption performance of TNAs as glucose biosensors [18,19]. Nevertheless, TNAs are prepared by adjusting the modification process, which has been reported in most studies so far, with no analysis having been carried out from the structure. Hence, defect processing and analysis of the intrinsic mechanism during the growth of TNAs have become important challenges in biosensors.

Here, we offer a strategy for preparing glucose biosensors with excellent selectivity, sensitivity and stability. TNAs-Air and TNAs-Ar were prepared by annealing under air and argon atmospheres, respectively. Among them, the surface of TNAs-Ar exhibits high activity, which is derived from the generation of a large number of oxygen vacancies, and can promote charge transfer and enzyme adsorption. Compared to TNAs-Air, the stability and selectivity of glucose biosensors based on TNAs-Ar were significantly improved.

## 2. MATERIALS AND METHODS

### *2.1 Reagents*

Pure titanium (thickness of 0.2 mm) was purchased from the Sumitomo Corporation of Japan. Glucose oxidase (GOD, 200 units/mg), ascorbic acid (AA), uric acid (UA) and dopamine (DA) were purchased from Sigma-Aldrich Co. In addition, a phosphate buffer solution (PBS) was composed of $Na_2HPO_4$ and $NaH_2PO_4$. Other chemicals and reagents, such as acetone, ethanol, NH4F, KCl, glucose, and chitosan (CS) were of analytical grade (Alibaba, Shanghai).

### *2.2 Preparation of TNAs*

The pure titanium was degreased, followed by sequential washing with acetone, deionized water and alcohol under ultrasonic conditions for 20 min. Then, an anodizing treatment was performed using an IPD-20001SLU-type regulated DC power supply and the specific process parameters were an electrolyte of 0.5 mol/L $NH_4F$ solution, a voltage of 50 V and an electrolysis time of 30 min. The sample was heated to 450°C at a ramp rate of 3°C/min and annealed in air and argon for 2 h, labeled as TNAs-Air and TNAs-Ar, respectively.

*2.3 Preparation of glucose biosensor*

The 5 μL 10 mg·mL$^{-1}$ GOD solution and the 10 μL 5 mg·mL$^{-1}$ CS solution were sequentially dispensed onto the surface of the prepared TNAs electrode, respectively, and dried in air to form a TNAs/GOD/CS electrode material. The prepared electrode was immersed in 0.1 M PBS (pH=6.8) to remove GOD without stable adsorption and then dried at room temperature, before being stored in a refrigerator at a temperature of 4 °C for the next step use.

*2.4 Characterization*

The crystalline structure of the TNAs were analyzed by X-ray diffractometry (XRD, D/MAX-3B). The TNAs microstructure was observed using scanning electron microscopy (SEM, VEGA-3SBH). Raman spectra were collected by a Raman microprobe with 514 nm (Bruker, RENISHAW). The elemental valence of the TNAs was determined by X-ray photoelectron spectroscopy (XPS, PHI-5000 Versa Probe II). The structural characteristics of the sample were detected by electron paramagnetic resonance (EPR, Bruker A300). UV-Vis absorption spectra of the samples were determined using a UV-Vis spectrophotometer (TU-1901). The electrochemical measurements were performed on an electrochemical workstation (CHI 760E).

## 3. RESULTS AND DISCUSSION

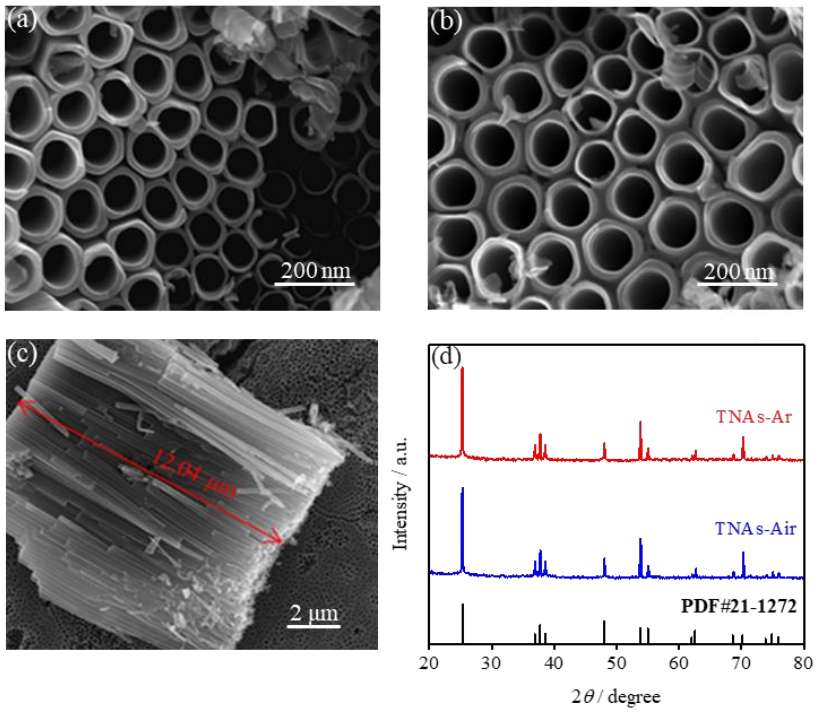


**Figure 1.** Phase composition and microstructure of TNAs-Air and TNAs-Ar: (a) SEM images of TNAs-Air; (b) SEM images of TNAs-Ar; (c) SEM cross-sectional images of TNAs-Ar; (d) XRD patterns of TNAs-Air and TNAs-Ar.

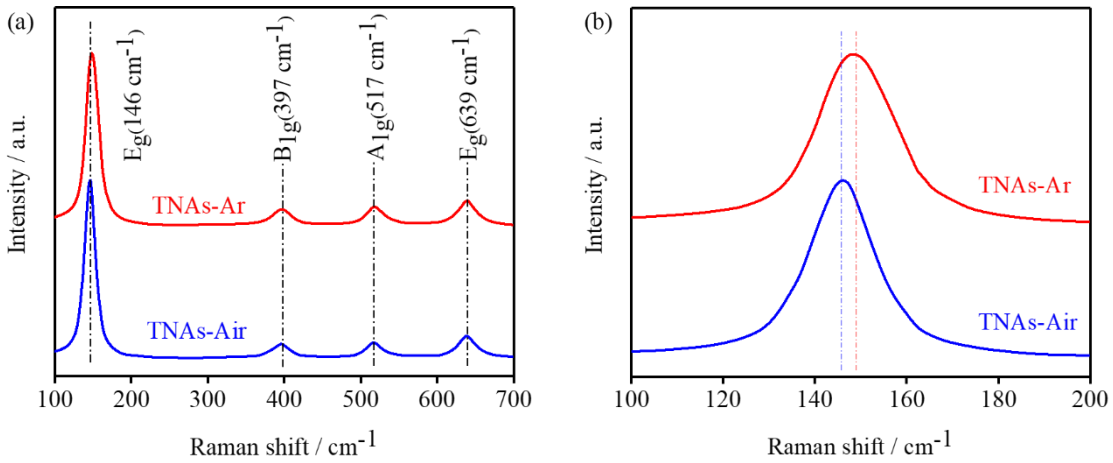


**Figure 2.** Raman spectra of TNAs-Air and TNAs-Ar.

The microstructure and phase composition of TNAs annealed in air and an argon atmosphere are shown in Fig.1. Figures 1a and b show the SEM images of TNAs-Air and TNAs-Ar (cross-sectional images as shown in Fig.1c), respectively. The structure of the TNAs that exhibits uniformity was not destroyed by annealing under the argon atmosphere.

TNAs-Ar can be up to 12.04 μm in length and have an average diameter of 155.3 nm. Interestingly, the XRD patterns of TNAs-Air and TNAs-Air (Fig.1d) exhibit a typical anatase structure (PDF#21-1272) and there are no significant changes in diffraction peak intensity and the full width at half maximum. The amorphous TNAs in the argon annealing atmosphere result in the generation of $Ti^{3+}$ ions and oxygen vacancies due to an insufficient oxygen supply [20]. Hence, TNAs with abundant oxygen vacancies are formed under argon annealing conditions.

Figure 2a shows the Raman spectra of TNAs in different annealing atmospheres, with the vibrational absorption peaks at 146, 397, 517 and 641 $cm^{-1}$ corresponding to anatase $TiO_2$ [20]. Compared with the TNAs-Air, the $E_g$ peak at 146 $cm^{-1}$ of TNAs-Ar undergoes broadened and a blue shift (Fig.2b). Studies by Salari [21] and Naldoni [22] have shown that the $E_g$ peak exhibits more sensitive properties to oxygen vacancies, and the presence of oxygen vacancies will result in changes in the peak shape and position of the $E_g$ peak in TNAs. Meanwhile, since the grain size of the sample did not change significantly (Fig.1), the broadening and blue shift of the $E_g$ peak of the Raman spectrum were due to the introduction of oxygen vacancies rather than the size effect. The above results indicate that oxygen vacancies can be introduced into TNAs under an argon atmosphere annealing treatment.

The effect of different annealing atmospheres on the chemical state of the samples can be observed clearly, with the XPS spectra of TNAs-Air and TNAs-Ar shown in Fig.3. Figure 3a shows that both TNAs-Air and TNAs-Ar consist of Ti, O and C elements, where C arises from contamination [23]. As can be seen, the peaks with binding energies at 458.02, 458.30, 463.57 and 464.32eV represent $Ti^{4+}$, while the peaks at 456.23 and 462.18 eV represent $Ti^{3+}$ (Figs.3b and d). It is noteworthy that $Ti^{3+}$ appears in TNAs-Ar, compared to TNAs-Air. Xing et al. confirmed that $Ti^{3+}$ production corresponds to the appearance of oxygen vacancies during annealing [24,25].

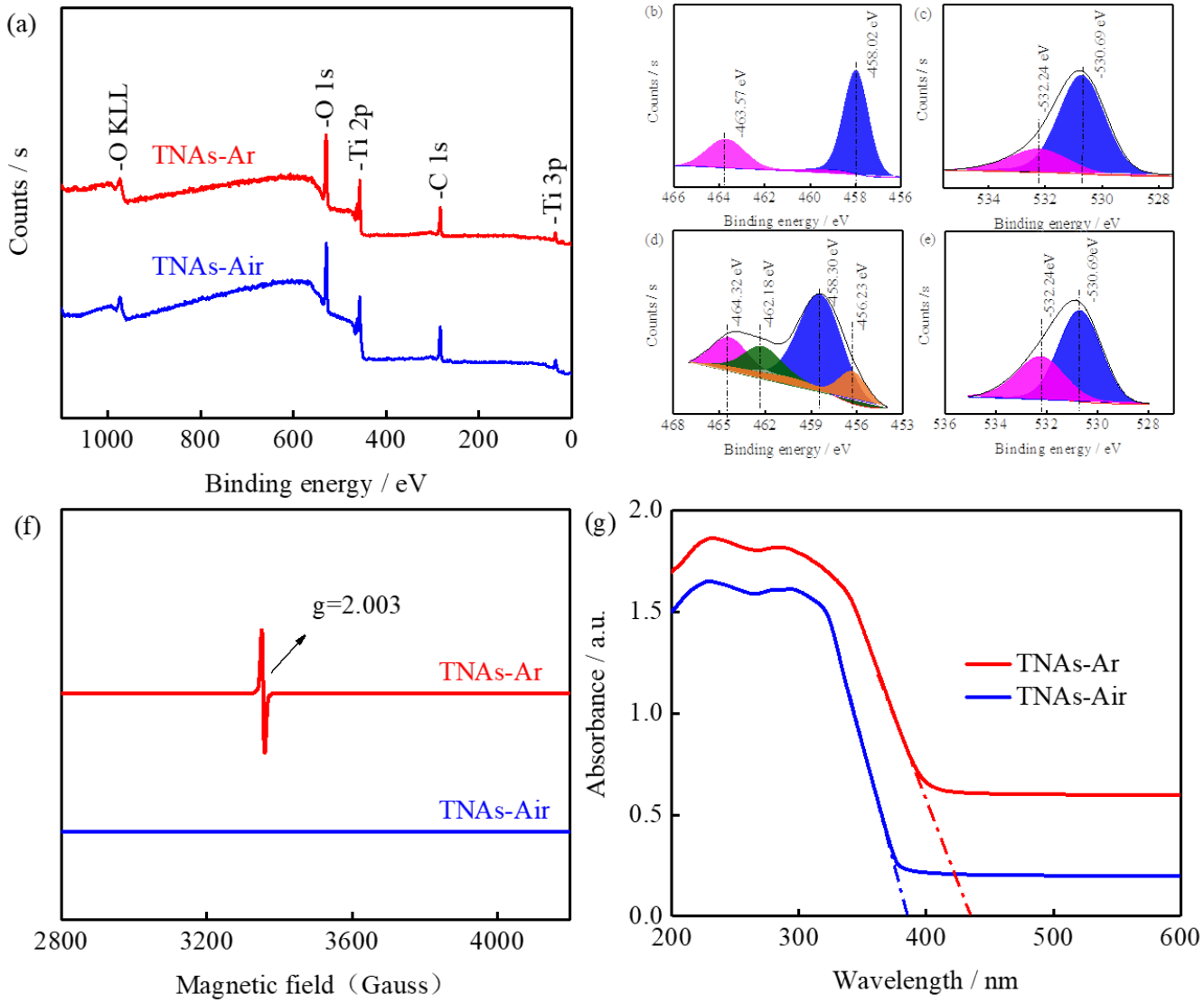


**Figure 3.** (a-e) XPS, (f) EPR and (g) UV/Vis spectra analysis of TNAs-Air and TNAs- Ar.

In addition, the peaks with binding energies at 530.69 eV represent $O^{2-}$ and the peaks at 532.24 eV represent $OH^-$. The O1s XPS spectra of TNAs-Air and TNAs-Ar are shown in Figs.3c and e, respectively. It can be seen that the peaks represented by $O^{2-}$ and $OH^-$ do not apparently shift, indicating that the surface species of TNAs undergo no change during different annealing atmospheres. To further demonstrate the presence of oxygen vacancies, the EPR spectra of TNAs samples at 123 K are shown in Fig.3f. Here, TNAs-Ar show a strong signal at g=2.003, which is due to the capture of electrons at the oxygen vacancies; thus, verifying the presence of oxygen vacancies on the TNAs-Air surface [26]. It was equally important to consider the rate of electron transport of samples. Due to the presence of oxygen vacancies and $Ti^{3+}$, the bandgap width of TNAs-Ar is 2.846 eV, which is 0.362 eV lower than TNAs-Air, which reduces the transmission barrier and increases the electron diffusion path (Fig. 3g) [27].

To study the GOD activity modified by the TNAs-Air and TNAs-Ar electrode materials, electrocatalytic experiments were carried out on the electrode materials. The cyclic voltammograms of the sample at 0.1 M and pH = 6.8 PBS (scanning rate of 100 mV $s^{-1}$) are shown in Fig.4. The peak

potential and current of TNAs-Air/GOX/CS and TNAs-Ar/GOX/CS electrodes in PBS do not significantly change, indicating that there was no significant difference in enzyme modification between the two electrodes. In addition, the peak potentials and peak currents of the TNAs-Air/GOX/CS and TNAs-Ar/GOX/CS electrodes do not change much, indicating that the TNAs-Air and TNAs-Ar electrodes have no significant difference in enzyme modification in PBS. However, when glucose was added to the solution, the TNAs-Air/GOX/CS electrode showed excellent electrocatalytic activity compared to the TNAs-Ar/ GOX/CS electrode, displaying that TNAs-Ar can provide more GOD adsorption. The site plays a greater role in bioelectrocatalysis.

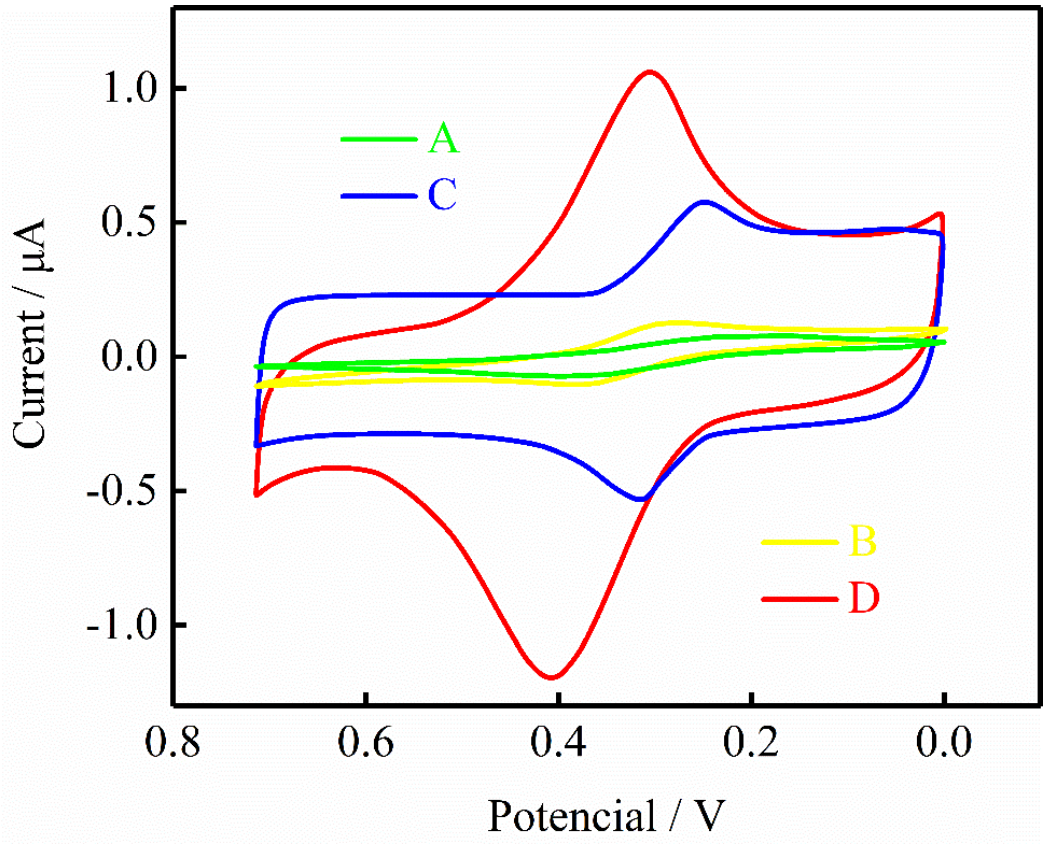


**Figure 4.** Cyclic voltammograms of TNAs-Air/GOD/CS and TNAs-Ar/GOD/CS electrodes in 0.1 M PBS (pH=6.8): (a) TNAs-Air/GOX/CS; (b) TNAs-Ar/GOX/CS; (c) TNAs-Air/GOX/CS and 1 mM glucose; (d) TNAs-Ar/GOX/CS and 1 mM glucose

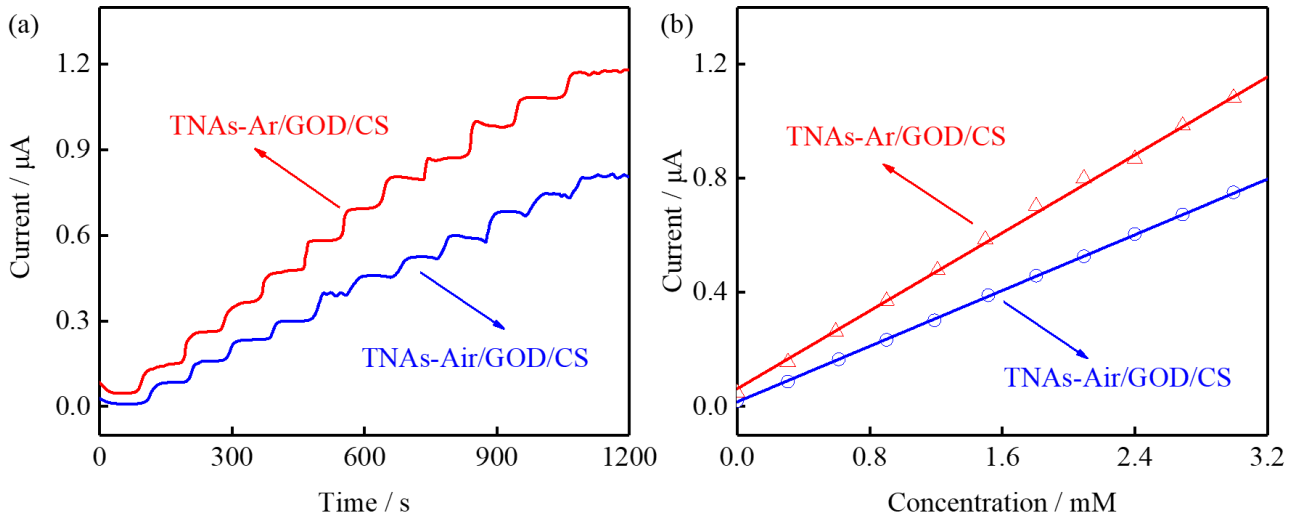


**Figure 5.** (a) Amperometric response of the TNAs-Air/GOD/CS and TNAs-Ar/GOD/CS in 0.1 M PBS with consecutive addition of various concentrations of glucose. (b) Linear fitting curve between current density and glucose concentrations.

Figure 5a shows the amperometric response of the TNAs-Air/GOD/CS and TNAs-Ar/GOD/CS electrodes with continuous addition of glucose to 0.1 M PBS (pH = 6.8) at 0.6 V. It can be clearly seen that as the glucose concentration increases, the current density increases at the TNAs-Air/GOD/CS and TNAs-Ar/GOD/CS electrodes, showing a fast response time of less than 10 s. Thus, those data reveal the rapid response and sensitivity of TNAs-Air/GOD/CS and TNAs-Ar/GOD/CS to glucose oxidation. Furthermore, the linear relationship between current density and glucose concentration for the TNAs-Air/GOD/CS and TNAs-Ar/GOD/CS electrodes is shown in Fig.5b. The TNAs-Air/GOD/CS and TNAs-Ar/GOD/CS electrodes show good linear current response to changes in glucose concentration, indicating that the reaction is a typical enzymatic kinetic reaction behavior. Meanwhile, the fitting equations for the current density and glucose concentration of the TNAs-Air/GOD/CS and TNAs-Ar/GOD/CS electrodes are shown in Eqs. (1) and (2):

$$j=0.040+0.611C \quad (1)$$

$$j=0.115+0.854C \quad (2)$$

where $j$ represents the response current density and C is the glucose concentration.

According to the fitting equation, the detection sensitivities of TNAs-Air/GOD/CS and TNAs-Ar/GOD/CS electrodes for glucose are 8.5 and 3.8 $\mu A \cdot mM^{-1}cm^{-2}$, respectively. Moreover, when S/N=3, the limits of detection of TNAs-Air/GOD/CS and TNAs-Ar/GOD/CS are 5.8 and 3.2 μM, respectively. The results show that the TNAs-Ar/GOD/CS electrode has higher detection sensitivity and lower limits of detection for glucose than the TNAs-Air/GOD/CS electrode. Meanwhile, both the sensitivity and the response time of TNAs-Ar/GOD/CS biosensor are superior to those of other metal oxide-based glucose biosensors, which are listed in Table 1.

**Table 1.** Comparison of analytical performance of metal oxide-based glucose biosensors.

| Electrode material | Sensor sensitivity ($\mu A \cdot mM^{-1} \cdot cm^{-2}$) | Response time (s) | Ref |
|---|---|---|---|
| TNAs-Ar/GOD/CS | 8.5 | <10 | This work |
| GOD/mesoporous $TiO_2$ | 3.9 | <10 | [28] |
| GOD/NiO hollow spheres | 3.4 | <10 | [29] |
| GOD/nanocrystalline $TiO_2$ | 4.6 | <30 | [30] |
| GOD/$TiO_2$-copolymer | 2.3 | <20 | [31] |

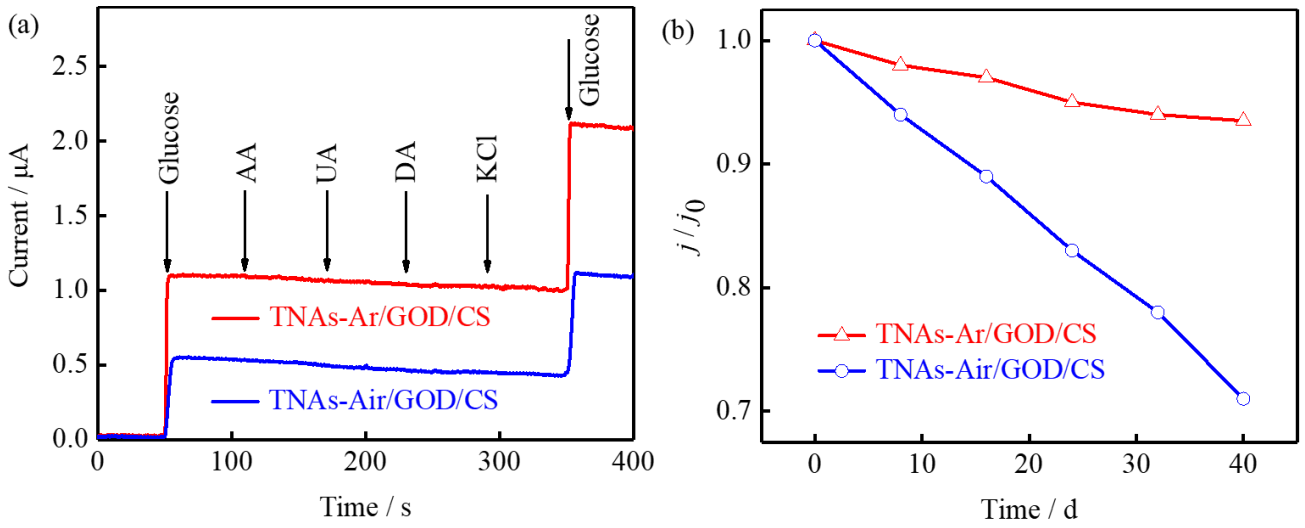


**Figure 6.** (a) Amperometric response of TNAs-Air/GOD/CS and TNAs-Ar/GOD/CS with consecutive additions of 1 mM glucose and 0.5 mM DA, UA, AA and KCl in 0.1M PBS. (b) Effect of current response of TNAs-Air/GOD/CS and TNAs-Ar/GOD/CS to 0.1 mM glucose in 0.1 MPBS for 40 d.

In order to verify the selectivity of the TNAs-Air/GOD/CS and TNAs-Ar/GOD/CS electrodes for glucose detection, we selected interfering substances, including AA, DA, UA and KCl, to interfere with the selectivity of glucose detection [28]. It is noteworthy that compared with the above interferent concentrations, the normal physiological level of glucose is higher, which is ~3–8 mM [29]. In this study, we investigated the continuous addition of glucose, AA, UA, DA, KCl (glucose: 1 mM; AA, DA, UA and KCl: 0.5 mM) in 0.1 M PBS with a working voltage of 0.6 V and a time interval of 60s amperometric responses. In the presence of interfering substances, the electrochemical response of glucose is shown in Fig.6a. It can be seen that TNAs-Ar/GOD/CS produces a stronger current response than the TNAs-Air/GOD/CS electrodes and the current response of the interferent is minimal. Among them, the high selectivity of the TNAs-Ar/GOD/CS electrodes is due to the large amount of active sites on the surface of TNAs annealed in the argon atmosphere, which provides a larger surface area for the

adsorption of GOD, greatly enriching the electrooxidation for glucose [30]. Simultaneously, in order to further verify the long-term stability of the TNAs-Air/GOD/CS and TNAs-Ar/GOD/CS electrodes, the current response of 1 mM glucose was detected every 5 d, and the sensor was stored in a refrigerator (4°C) when not in use. The 40-d response current response of the TNAs-Air/GOD/CS and TNAs-Ar/GOD/CS electrodes to 1 mM glucose in 0.1 M PBS is shown in Fig.6b. After 40 days, the TNAs-Ar/GOD/CS electrode retained 93.5% of the initial current response. The experimental results show that the prepared sensor has excellent performance and good selectivity and stability.

To evaluate the practicality of the TNAs-Ar/GOD/CS electrode, we selected the glucose in human blood serum for testing. Human blood serum was collected from hospitalized patients and the glucose concentration was pre-determined to be 5.1 mM by a ROCHE COBAS C 111 analyzer, with 1 mL of serum was diluted to 10 mL by adding PBS (pH 7.0). The glucose in human blood serum samples were determined using TNAs-Ar/GOD/CS by amperometry. The comparison of the added values and the determined values were listed in Table 1. The added glucose shows the good recoveries from 98.7 to 103.2%. The good recoveries achieved in glucose reveal the appreciable practicality of the TNAs-Ar/GOD/CS sensor. Thus, the above results reveal excellent practical feasibility of the prepared TNAs-Ar/GOD/CS sensor for the determination of glucose.

**Table 2.** Determination of glucose in human serum samples with TNAs-Ar/GOD/CS.

| Samples | Added (mM) | Found (mM) | RSD (%) | Recovery (%) |
|---|---|---|---|---|
| 1 | 0.050 | 0.578 | 2.4 | 103.2 |
| 2 | 0.200 | 0.708 | 2.8 | 99.7 |
| 3 | 0.500 | 1.009 | 2.9 | 99.9 |
| 4 | 1.000 | 1.518 | 2.6 | 100.5 |
| 5 | 2.000 | 2.477 | 3.0 | 98.7 |

## 4. CONCLUSIONS

In this paper, by engineering the defects in TNAs through argon annealing, the adsorption activity can be increased effectively. More importantly, the correlation between the surface defect engineering and the macroscopic properties of enzymatic glucose biosensors was established by using TNAs-Ar. Also, our work provides a new strategy for the basic defect theory of TNAs. Meanwhile, the method studied here to introduce oxygen vacancies in $TiO_2$ can be further applied to other forms of $TiO_2$ to enhance their adsorption properties. In addition, the oxygen vacancies generated by annealing under an argon atmosphere may introduce more interesting properties, including photocatalys is and electrochemistry, into the TNAs.

## References

1. B.D. Malhotra and A. Chaubey, *Sensor. Actuat. B-Chem.*, 91 (2003) 117-127.
2. B. Liang, L. Li, X. Tang, Q. Lang, H. Wang, F. Li, J. Shi, W. Shen, I. Palchetti, M. Mascini and A.

Liu, *Biosens. Bioelectron.*, 45 (2013) 19-24.
3. E.B. Bahadirand M.K. Sezginturk, *Anal. Biochem.*, 478 (2015) 107-120.
4. M. Baghayeri, A. Amiri and S. Farhadi, *Sensor. Actuat. B-Chem.*, 225 (2016) 354-362.
5. Q. Liu, Y. Liu, F. Wu, X. Cao, Z. Li, M. Alharbi, A.N. Abbas, M.R. Amerand C. Zhou, *ACS Nano*, 12 (2018) 1170-1178.
6. W.W. Zhao, J.J. Xu and H.Y. Chen, *Biosens. Bioelectron.*, 92 (2017) 294-304.
7. K. Mondal, M.A. Ali, C. Singh, G. Sumana, B.D. Malhotra and A. Sharma*Sensor. Actuat. B-Chem.*, 246 (2017) 202-214.
8. S. Kumar, W. Ahlawat, R. Kumarand N. Dilbaghi, *Biosens. Bioelectron.*, 70 (2015) 498-503.
9. L. Wu, S. Wu, Z. Xu, Y. Qiu, S. Li and H. Xu, *Biosens. Bioelectron.*, 80 (2016) 59-66.
10. Y. Shen, Y. Zhang, X. Zhang, X. Zhou, X. Teng, M. Yan and H. Bi, *Nanoscale*, 7 (2015) 2941-2950.
11. M. Zhou, A.M. Glushenkov, O. Kartachova, Y. Li and Y. Chen, *J. Electrochem. Soc.*, 162 (2015) A5065-A5069.
12. L. Li, J. Yan, T. Wang, Z.J. Zhao, J. Zhang, J. Gong and N. Guan, *Nat. Commun.*, 6 (2015) 5881.
13. R.A. Doong and H.M. Shih, *Biosens. Bioelectron.*, 25 (2010) 1439-1446.
14. M. Abdullah and S.K. Kamarudin, *Renew. Sust. Energ. Rev.*, 76 (2017) 212-225.
15. G. Davis, *Biosens*, 2 (1986) 101-124.
16. J.M. Macak, H. Tsuchiya and P. Schmuki, *Angew. Chem. Int. Edit.*, 44 (2005) 2100-2102.
17. T. Close, G. Tulsyan, C.A. Diaz, S.J. Weinstein and C. Richter, *Nat. Nanotechnol.*, 10 (2015) 418-422.
18. S. Sakthivel and H. Kisch, *Angew. Chem. Int. Edit.*, 42 (2003) 4908-4911.
19. X. Chenand S.S. Mao, *Chem. Rev.*, 107 (2007) 2891-2959.
20. H. Wu, D. Li, X. Zhu, C. Yang, D. Liu, X. Chen, Y. Song and L. Lu, *Electrochim. Acta*, 116 (2014) 129-136.
21. M. Salari, K. Konstantinov and H.K. Liu, *J. Mater. Chem.*, 21 (2011)5128-5133.
22. A. Naldoni, M. Allieta, S. Santangelo, M. Marelli, F. Fabbri, S. Cappelli, C.L. Bianchi, R. Psaro and V. Dal Santo, *J. Am. Chem. Soc.*, 134 (2012) 7600-7603.
23. J. Fang, F. Wang, K. Qian, H. Bao, Z. Jiangand W. Huang, *J. Phys. Chem. C*, 112 (2008) 18150-18156.
24. M. Xing, W. Fang, M. Nasir, Y. Ma, J. Zhang and M. Anpo, *J. Catal.*, 297 (2013) 236-243.
25. M. Xing, J. Zhang, F. Chen and B. Tian, *Chem. Commun.*, 47 (2011) 4947-4949.
26. S. Wang, L. Pan, J.J. Song, W. Mi, J.J. Zou, L. Wang and X. Zhang, *J. Am. Chem. Soc.*, 137 (2015) 2975-2983.
27. Y. Yan, T. Lei,Y. Jiao,C. Wu and J. Xiong. *Electrochim. Acta*, 264(2018) 20-25.
28. S.J. Bao, C.M. Li, J.F. Zang, X.Q. Cui, Y. Qiao and J. Guo, *Adv. Funct. Mater.*, 18 (2008) 591-599.
29. C. Li, Y. Liu, L. Li, Z. Du, S. Xu, M. Zhang, X.M. Yin and T.H. Wang, *Talanta*, 77 (2008) 455-459.
30. Q. Li, G. Luo, J. Feng, Q. Zhou, L.I. Zhang and Y. Zhu, *Electroanal.*, 13 (2001) 413-416.
31. X. Chen and S. Dong, *Biosens. Bioelectron.*, 18 (2003) 999-1004.
32. S. Yang, G. Li, D. Wang, Z. Qiao and L. Qu, *Sensor. Actuat. B-Chem.*, 238 (2017) 588-595.
33. P. Moozarm Nia, W.P. Meng, F. Lorestani, M.R. Mahmoudianand Y. Alias, *Sensor. Actuat. B-Chem.*, 209 (2015) 100-108.
34. Y. Song, C. Zhu, H. Li, D. Du and Y. Lin, *RSC Adv.*, 5 (2015) 82617-82622.